

Article

Novel Sodium Alginate/Polyvinylpyrrolidone/TiO₂ Nanocomposite for Efficient Removal of Cationic Dye from Aqueous Solution

Noha A. Elessawy ^{1,*}, Marwa H. Gouda ¹, Mohamed S. Elnouby ¹, Hoda F. Zahran ², Aly Hashim ¹,
Mona M. Abd El-Latif ¹ and Diogo M. F. Santos ^{3,*}

¹ Advanced Technology and New Materials Research Institute (ATNMRI), City of Scientific Research and Technological Applications (SRTA-City), New Borg El-Arab City, Alexandria P.O. Box 21934, Egypt; mgouda@srtacity.sci.eg (M.H.G.); melnouby@srtacity.sci.eg (M.S.E.); ahashem@srtacity.sci.eg (A.H.); mabdellatif@srtacity.sci.eg (M.M.A.E.-L.)

² Environment and Natural Materials Research Institute, City of Scientific Research and Technological Applications (SRTA-City), New Borg El-Arab City, Alexandria P.O. Box 21934, Egypt; hzahran@srtacity.sci.eg

³ Center of Physics and Engineering of Advanced Materials (CeFEMA), Instituto Superior Técnico, Universidade de Lisboa, 1049-001 Lisbon, Portugal

* Correspondence: nelessawy@srtacity.sci.eg (N.A.E.); diogosantos@tecnico.ulisboa.pt (D.M.F.S.)

Featured Application: Novel SA/PVP/TiO₂ nanocomposite beads can be used as an effective, eco-friendly adsorbent-photocatalyst for treating cationic dye-contaminated wastewaters.



Citation: Elessawy, N.A.; Gouda, M.H.; Elnouby, M.S.; Zahran, H.F.; Hashim, A.; Abd El-Latif, M.M.; Santos, D.M.F. Novel Sodium Alginate/Polyvinylpyrrolidone/TiO₂ Nanocomposite for Efficient Removal of Cationic Dye from Aqueous Solution. *Appl. Sci.* **2021**, *11*, 9186. <https://doi.org/10.3390/app11199186>

Academic Editor: Adina Magdalena Musuc

Received: 6 September 2021

Accepted: 30 September 2021

Published: 2 October 2021

Publisher's Note: MDPI stays neutral with regard to jurisdictional claims in published maps and institutional affiliations.



Copyright: © 2021 by the authors. Licensee MDPI, Basel, Switzerland. This article is an open access article distributed under the terms and conditions of the Creative Commons Attribution (CC BY) license (<https://creativecommons.org/licenses/by/4.0/>).

Abstract: The combination of adsorption and photodegradation processes is an effective technique for the removal of dye contaminants from water, which is motivating the development of novel adsorbent-photocatalyst materials for wastewater treatment. Herein, novel nanocomposite porous beads were developed using titanium dioxide (TiO₂) nanotubes embedded in a sodium alginate (SA)/polyvinylpyrrolidone (PVP) matrix using calcium chloride solution as a crosslinker. The prepared nanocomposite beads' performance was examined as an adsorbent-photocatalyst for the breakdown of methylene blue in aqueous solutions. Several operation factors influencing the dye decomposition process, including photocatalyst dosage, illumination time, light intensity, and stability were investigated. The findings demonstrated that the removal activity of the beads changed with the TiO₂ weight ratio in the composite. It was found that SA/PVP/TiO₂-3 nanocomposite beads presented the greatest deterioration efficiency for methylene blue dye (98.9%). The cycling ability and reusability of the prepared SA/PVP/TiO₂ nanocomposite beads recommend their use as efficient, eco-friendly materials for the treatment of wastewaters contaminated with cationic dyes.

Keywords: hydrogel nanocomposite beads; sodium alginate; polyvinylpyrrolidone; cationic dye; photodegradation

1. Introduction

The release of dye-contaminated wastewaters from different industries [1] into the environment leads to dramatic effects on the living life of our planet, as dyes and their sub-products are often toxic or mutagenic agents [2]. Different techniques are used to treat waters polluted with dyes, such as adsorption [3,4], photocatalysis [5], biological methods [6,7], coagulation, and flocculation [8].

Recently, photocatalysis degradation has been used widely to remove several organic [9] and inorganic [10] wastewater contaminants by transforming them into non-hazardous materials. One of the semiconductor materials most commonly utilized as a photocatalyst to remove various contaminants from wastewaters is titanium dioxide (TiO₂), which was studied as a photocatalyst for the first time in 1972 by Fujishima and Honda [11]. TiO₂ is a non-toxic and bio-friendly material, chemically stable, photostable, commercially

available with a low cost price, has high transparency to visible light, and can be activated with sunlight or UV radiation [12,13]. The problem regarding the application on an industrial scale of TiO₂ nanostructures is the low adsorption of organic pollutants, uniform distribution of nanoparticles, and the sluggish separation and recovery of nanosized particles during the process of wastewater treatment. Supporting TiO₂ nanostructures on a polymeric matrix can overcome this difficulty.

TiO₂ incorporated into a calcium (Ca)-alginate film matrix was used as a photocatalyst to remove methyl orange with 82.2% effectiveness after 120 min of UV irradiation [14]. ZnO and TiO₂ nanoparticles embedded into Ca-alginate beads were also used as a photocatalyst to remove copper ions [10]. By using cross-linked sodium alginate (SA) with TiO₂, forming a SA–TiO₂ hydrogel, an adsorption efficiency for methyl violet dye of 99.6% was reported, whereas SA-based film only achieved 85%. This effect was attributed to the electrostatic attraction between the methyl violet dye and TiO₂, which behaves as an anionic center in the hybrid hydrogel [15]. On the other hand, after two cycles of reuse, the SA–TiO₂ hybrid film was still effective in degrading Congo red under UV light, with no appreciable loss of catalytic activity [16]. Generally, adsorption-photocatalytic degradation of dyes is favored using TiO₂; however, a high concentration of dye solution can hinder the photocatalytic activity of TiO₂ due to its surface saturation. Besides, the dye molecules are prone to absorb light energy. As a result, the production of reactive oxygen species and hydroxyl radicals is reduced.

SA is a brown seaweed-derived natural polysaccharide polymer. It is a non-toxic, biocompatible, and biodegradable polymer composed of two acids, namely α -L-guluronic and β -D-mannuronic acid. SA is suitable for chemical modification and can be shaped as hydrogel beads by cross-linking the α -L-guluronic acid units with poly- or divalent cations [17,18]. It is frequently employed as a polymeric matrix that can support catalysts [10]. To overcome the natural polymer's drawbacks, such as microbial breakdown and low mechanical strength, SA was blended with synthetic polymers, including polyvinyl alcohol (PVA) [19], polyethylene glycol (PEG), and polyethylene oxide (PEO) [20]. The inclusion of active functional groups on natural and synthetic polymers in the polymeric network allows the hydrogel beads to be used efficiently as adsorbents as a result of the blending [21].

In this study, to improve the porosity of the produced beads, polyvinylpyrrolidone (PVP) was combined with SA as a natural pore-forming polymer [22]. In addition, TiO₂ nanotubes were incorporated into SA/PVP polymer matrix to yield novel SA/PVP/TiO₂ nanocomposite beads using calcium chloride (CaCl₂) as the cross-linker. The main objective was to obtain a novel hybrid nanocomposite material having adsorption-photocatalyst activity by a simple, cheap, and efficient method. Its photocatalytic activity was investigated for the removal of cationic dyes, namely methylene blue (MB), from aqueous solutions. This nanocomposite overcomes the drawbacks of typical suspended solutions containing TiO₂ nanoparticles, which cause secondary pollution in the water treatment process.

2. Materials and Methods

2.1. Materials

Sodium alginate (SA), polyvinylpyrrolidone (PVP), and titanium (IV) dioxide rutile powder (TiO₂, <5 μ m) were all acquired from Sigma Aldrich. All compounds were used without further purification, and the solutions were made with deionized water.

2.2. Preparation of Polymeric Beads

Each polymer was individually dissolved at 25 °C in deionized water and mixed for 2 h in a mixture comprising 90 wt.% SA, 9–7 wt.% PVP, and 1–3 wt.% TiO₂ nanotubes, prepared from previous work [23], to form homogenous solutions. Using a syringe, the polymer mixture was then added dropwise into a 2% (*w/v*) CaCl₂ solution. After shaping the beads, they were rinsed three times with distilled water.

Figure 1 shows the possible structure of SA/PVP/TiO₂ nanocomposite beads, where the two polymers are crosslinked through acid-base interaction between carboxylic groups of SA and amine groups of PVP, in addition to the hydrogen bonds formed between the oxygenated groups of the polymers' molecules and the TiO₂ doping agent.

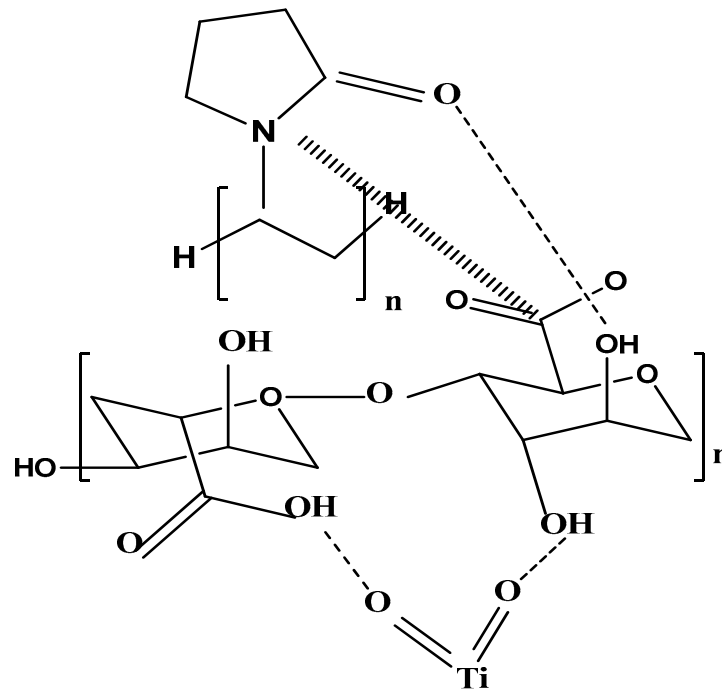


Figure 1. Possible structure of the SA/PVP/TiO₂ nanocomposite.

2.3. Characterization

The crystallographic phases of the produced samples were determined by X-ray powder diffraction (XRD, Shimadzu-7000, Kyoto, Japan). The elements were identified using transmission electron microscopy (TEM, JEM-2100 plus) and scanning electron microscopy (SU-70, Hitachi, Japan) in combination with energy-dispersive X-ray spectroscopy (EDS). A Bruker ALPHA spectrometer (Bruker Corporation, Rheinstetten, Germany) was used to perform the Fourier transform infrared (FTIR) study.

2.4. Photocatalytic Decay of Methylene Blue

Under illumination of an unfiltered commercial LED visible light, specifically two 12 W lamps with 1200 lm (Bareeq, Egypt), the photocatalytic degradation of MB dye was assessed using two loading ratios of doping agent in the SA/PVP polymer matrix. Typically, 1 g L⁻¹ of the SA/PVP/TiO₂ nanocomposite beads was suspended in MB dye solution model wastewater. The suspension was agitated at 25 °C using magnetic stirring under visible light, and samples were taken at regular intervals. A UV-vis spectrophotometer (Shimadzu UV-2600, Kyoto, Japan) was used to evaluate the residual MB concentration after irradiation by sampling 3 mL of the reaction mixture at the wavelength of 665 nm. The photocatalytic decay of MB was calculated by means of Equation (1),

$$\text{photodegradation (\%)} = [(C_0 - C) / C_0] \times 100 \quad (1)$$

where C_0 and C stand for the initial and final MB dye concentration, respectively.

The photocatalytic efficiency of the produced nanocomposite beads on MB dye degradation was investigated at a pH of 7. This pH value is the most suited for photocatalytic degradation [24] and was set by adding either 0.1 M NaOH or 0.1 M HCl solution.

2.5. Kinetic Models

The most widely used kinetic models are the pseudo-first order and pseudo-second order models [1]. The pseudo-first order model is given by Equation (2),

$$\log(q_e - q_t) = \log q_e - K_1 t \quad (2)$$

where q_e and q_t represent the MB adsorption capacity (mg g^{-1}) (i.e., the quantity of MB dye adsorbed or degraded) at equilibrium and at time t (s), respectively, and K_1 represents the rate constant (s^{-1}). The plots of $\log(q_e - q_t)$ vs. t enable determining the K_1 values. Equation (3) describes the pseudo-second order model,

$$\frac{t}{q_e} = \frac{1}{K_2 q_e^2} + \left(\frac{1}{q_e}\right)t \quad (3)$$

where K_2 ($\text{g mg}^{-1} \text{s}^{-1}$) represents the rate constant of the pseudo-second order model. When pseudo-second order kinetics is adopted, the plot of t/q_t vs. t should show a linear relation. The slope and intercept of the plot can be used to obtain q_e and K_2 , respectively.

3. Results and Discussion

3.1. Characterization of SA/PVP/TiO₂ Nanocomposite

The TEM image of TiO₂ shown in Figure 2a proves the formation of the tubular shape with nanoscale size. After the TiO₂ nanotubes were embedded in the blended SA/PVP polymers, SA/PVP/TiO₂ nanocomposite beads were obtained, as confirmed from EDS data (Figure 2b). As shown in the SEM micrograph of Figure 2c, the beads presented a rough and wrinkled morphology. By taking a higher magnification SEM image, a good dispersion of the TiO₂ nanotubes was observed with visible pores in the polymer matrix (Figure 2d).

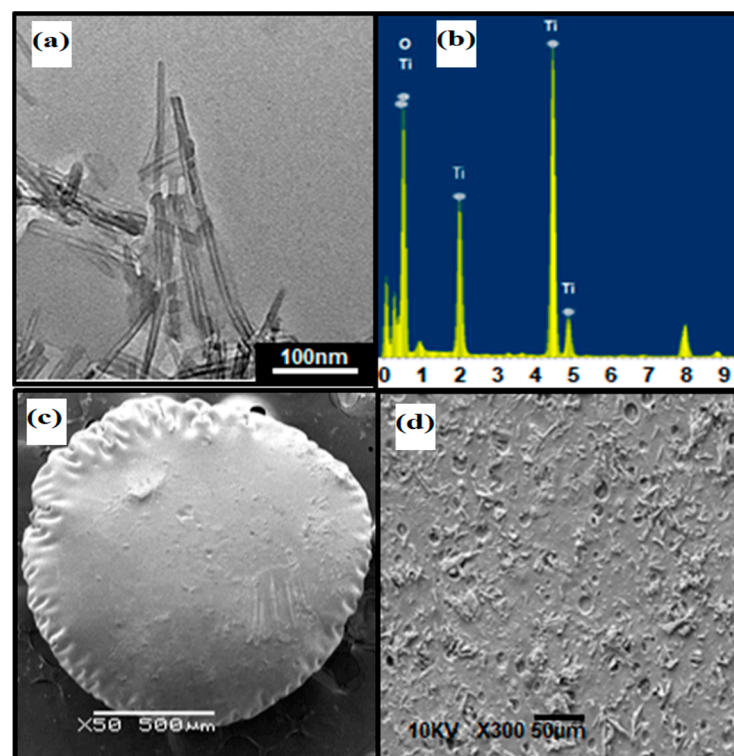


Figure 2. (a) TEM image of the TiO₂ nanotube and (b) EDS data of SA/PVP/TiO₂ nanocomposite. SEM micrographs of the (c) spherical-shaped bead and (d) higher magnification of bead's surface.

The FTIR spectra of TiO₂ nanotubes and SA/PVP/TiO₂ nanocomposite are shown in Figure 3. The band at about 500 cm⁻¹ for the TiO₂ nanotube seen in Figure 3a is characteristic of Ti-O stretching vibration modes. The FTIR spectra of SA/PVP/TiO₂ nanocomposite samples exhibit bands around 1600 cm⁻¹ assigned to O-H stretching mode, as well as absorption bands at 1419 cm⁻¹ ascribed to COO symmetric stretching vibration in SA. The band at 1030 cm⁻¹ corresponds to C-O stretching [25], the band at 2178 cm⁻¹ is related to PVP's C-N bond stretching vibration, and the band located at 2170–2300 cm⁻¹ represents the polymers' C-H bonds' bending vibration [22].

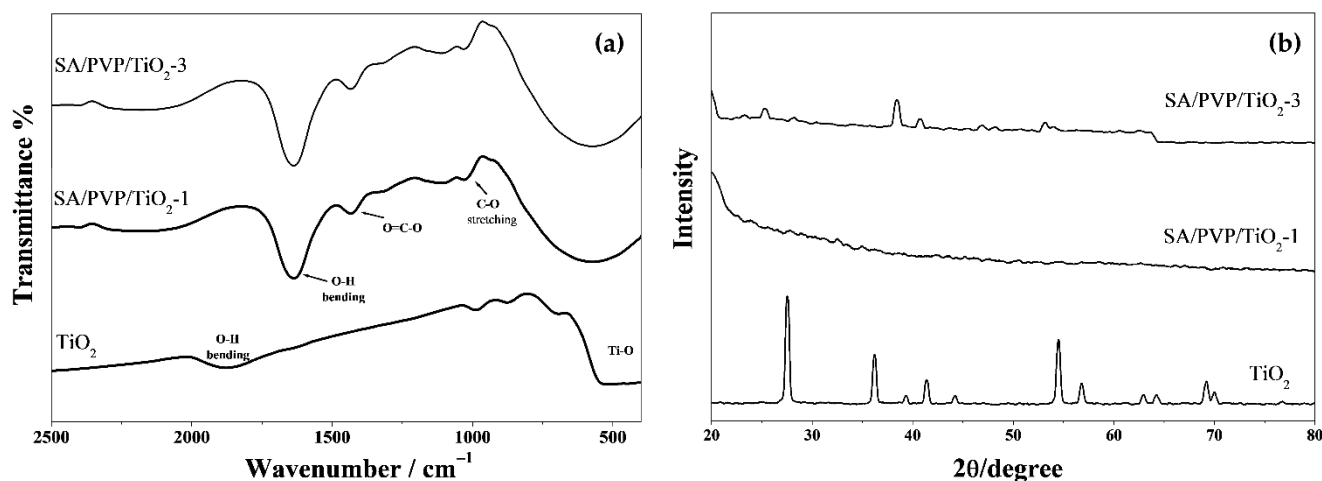


Figure 3. (a) FTIR spectra and (b) XRD spectra of the TiO₂ nanotubes and SA/PVP/TiO₂ nanocomposite beads.

The XRD patterns in Figure 3b show the crystalline features of TiO₂ nanotubes, with characteristic peaks at 2θ values of 28, 36, 41, and 54, whereas characteristic spectra of an amorphous structure are obtained for the prepared beads. The amorphous nature of the nanocomposites is related to the low Ti content (e.g., 2.7 wt.% Ti in SA/PVP/TiO₂-3), as determined by EDS analysis.

3.2. Adsorption and Photocatalytic Removal of MB

3.2.1. Effect of TiO₂ Amount in the SA/PVP Matrix

As the catalyst loading in the SA/PVP/TiO₂ nanocomposite has a key role in dye decay efficiency, the effect of the photocatalyst concentration on MB degradation was investigated by increasing the TiO₂ amount in the SA/PVP matrix from 1 to 5 wt.%. As seen in Figure 4, the decay efficiency rose when the TiO₂ concentration increased from 1 to 3 wt.%, which can be justified by the fact that at low concentrations, more porous empty sites and polymer functional groups, such as COO, are accessible on the beads' external surface to absorb cationic dye molecules via electrostatic attraction. However, the active sites available for the photocatalytic reaction are limited. Thus, by increasing the catalyst loading to 3 wt.%, additional active sites become available for the photocatalytic reaction. This leads to an increase in the hydroxyl ions' adsorption onto the surface of the beads to produce OH[•] radicals. On the other hand, the photocatalytic activity decreased at a high concentration of the catalyst, as it hampers the dye decay rate as a result of light penetration shortage inside the beads. A second possibility is the agglomeration of the catalyst nanoparticles, resulting in a decrease in the operative surface area of the catalyst, and consequently, a decrease in the decolorization efficiency.

3.2.2. Effect of Illumination Time on the Decay of MB

The activity of the prepared SA/PVP/TiO₂ nanocomposites was investigated in a dark environment to assess the level of MB dye adsorption in the beads. These data were used to evaluate the photocatalytic activity of SA/PVP/TiO₂ nanocomposites for eliminating MB dye in the presence of visible light. The experiments were carried out using 1 g L⁻¹ of

one of the two studied concentrations of doping agent (1 and 3 wt.% of TiO₂, respectively for SA/PVP/TiO₂-1 and SA/PVP/TiO₂-3 nanocomposite beads) in a 500 mL solution containing 50 mg L⁻¹ of MB dye at pH 7. The analysis was done at different time intervals in the dark and under visible light. As illustrated in Table 1, the dark adsorption increased with time and stabilized after 40 min, indicating that the active site and porosity of the SA/PVP blended polymer were saturated with MB molecules. Furthermore, carboxylic groups are the prevalent functional groups in the SA polymer, aiding in the adsorption of the cationic dye molecules.

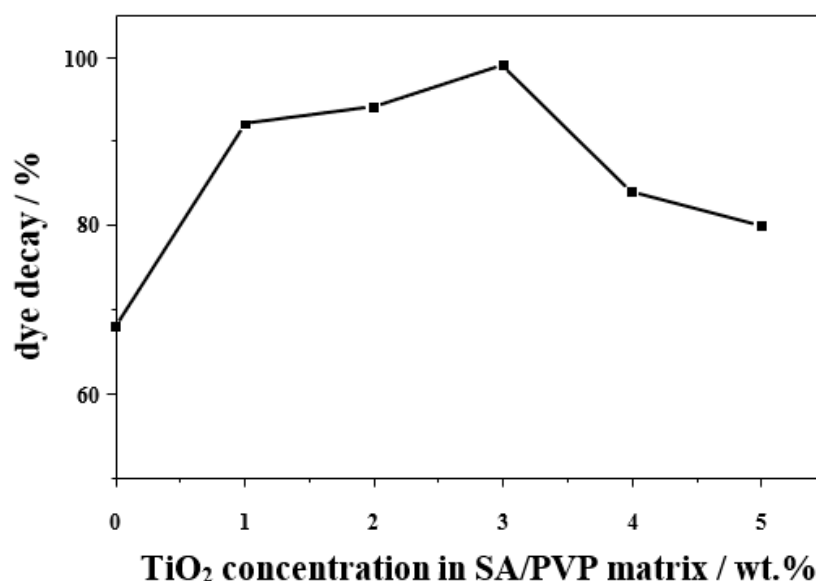


Figure 4. The influence of catalyst loading on dye degradation (pH 7; illumination time: 120 min; initial MB concentration: 50 mg L⁻¹; and light intensity: 1200 lm).

Table 1. Experimental data * on the effect of illumination time on MB dye degradation (%) using SA/PVP/TiO₂ nanocomposite beads.

Time (min)	Dye Removal % with SA/PVP/TiO ₂ -1 in Dark	Dye Removal % with SA/PVP/TiO ₂ -3 in Dark	Dye Removal % with SA/PVP/TiO ₂ -1 in Light	Dye Removal % with SA/PVP/TiO ₂ -3 in Light
10	21.0 ± 0.1	20.0 ± 0.1	23.9 ± 0.1	26.4 ± 0.1
20	39.0 ± 0.1	38.0 ± 0.1	41.0 ± 0.1	48.7 ± 0.1
30	48.0 ± 0.1	49.3 ± 0.1	58.6 ± 0.1	63.5 ± 0.1
40	58.0 ± 0.1	58.1 ± 0.1	67.0 ± 0.1	72.0 ± 0.1
50	58.6 ± 0.1	58.8 ± 0.1	70.3 ± 0.1	79.1 ± 0.1
60	58.9 ± 0.1	59.0 ± 0.1	78.9 ± 0.1	85.2 ± 0.1
70	59.3 ± 0.1	59.0 ± 0.1	84.4 ± 0.1	90.7 ± 0.1
80	59.5 ± 0.1	59.6 ± 0.1	88.0 ± 0.1	94.3 ± 0.1
90	59.8 ± 0.1	59.9 ± 0.1	91.3 ± 0.1	98.2 ± 0.1
100	59.9 ± 0.1	60.0 ± 0.1	91.6 ± 0.1	98.4 ± 0.1
110	60.0 ± 0.1	60.3 ± 0.1	91.8 ± 0.1	98.8 ± 0.1
120	60.2 ± 0.1	60.1 ± 0.1	92.1 ± 0.1	98.9 ± 0.1

* average values according to 3 replicates.

However, under visible light, as can be seen in Figure 5, the results reveal that the photocatalytic activity increased with the duration of the illumination period, with the SA/PVP/TiO₂-1 and SA/PVP/TiO₂-3 nanocomposite beads reaching 92% and 98.9% of MB dye decay, respectively, after 120 min of illumination.

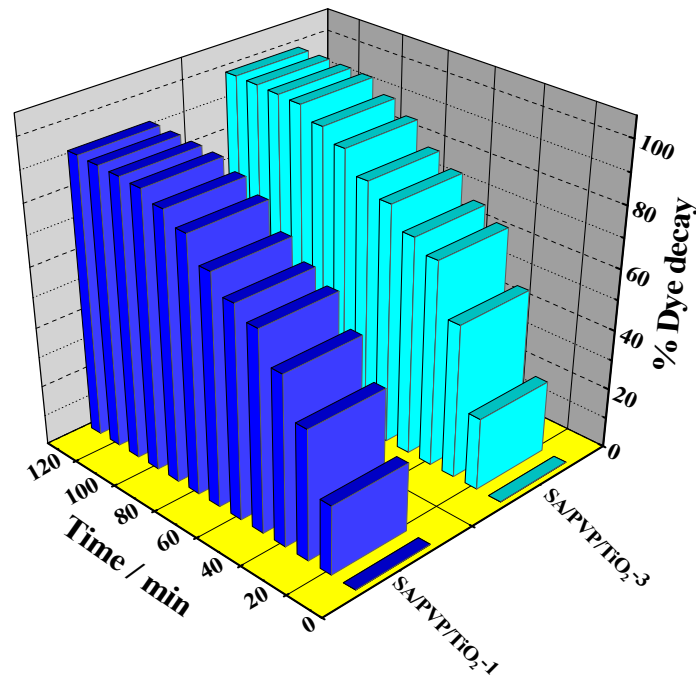


Figure 5. Effect of the illumination time in the degradation of methylene blue (%) in light using the SA/PVP/TiO₂ nanocomposites beads.

3.2.3. Effect of Light Intensity on MB Photocatalytic Degradation

The influence of light intensity on the efficiency of photocatalytic MB dye decay was evaluated using two concentrations of TiO₂. The intensity of the light over the system was varied by holding either one or two lamps on the reactor cover. As shown in Figure 6, the efficiency of the system after 120 min was enhanced by increasing the light intensity. This suggests that for higher intensity, the amount of light reaching the photocatalyst particles increases, thus increasing electron stimulation and the efficiency of the system [26].

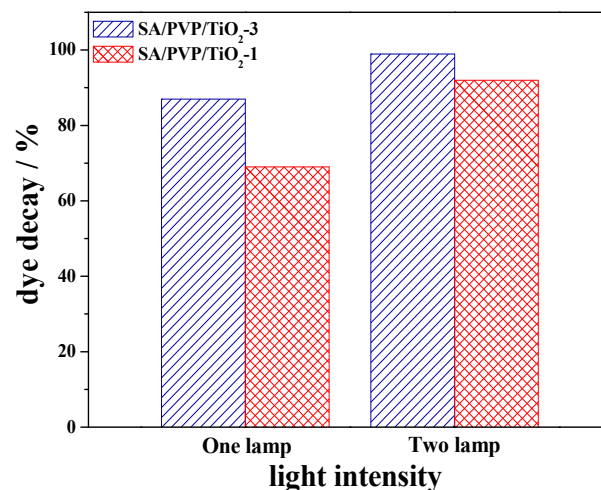


Figure 6. Effect of the light intensity on MB photocatalytic degradation using SA/PVP/TiO₂ nanocomposite (pH 7; 120 min of illumination time; and 50 mg L⁻¹ initial MB concentration).

3.2.4. Effect of the MB Dye Initial Concentration on its Photocatalytic Decay

The effect of the initial dye concentration on the photocatalytic decay of MB is shown in Figure 7 for both SA/PVP/TiO₂-1 and SA/PVP/TiO₂-3 nanocomposite beads. In each experiment, the same quantity of nanocomposite beads (1 g L⁻¹) was added to solutions containing different dye concentrations (10, 25, 50, and 100 mg L⁻¹). The pH of the

dye solution was kept at 7 and the contact time and light intensity were 120 min and 1200 lm, respectively. Figure 7 shows that dye decay tends to increase for higher initial MB concentration, the higher decay being attained at 50 mg L⁻¹. Further increasing the MB dye concentration negatively affected its decay. This can be justified by the dependence of the photodegradation rate of the dyes on the formation of OH• radicals on the catalyst surface, followed by the reaction of such radicals with the MB dye molecules. The higher dye decay rate observed at lower initial dye concentrations can be related to a higher chance of the dye molecules to react with OH• [27,28]. The following steps describe the mechanism proposed for MB degradation via the nanocomposite beads. First, irradiation with visible light enables electrons in the valence band to move to the conduction band. The surface of the TiO₂ photocatalyst then forms holes and electrons. Electrons react with dissolved O₂ to produce O₂^{•-}, while holes react with OH⁻ ions to produce OH•. The latter reacts with MB dye to degrade it into non-toxic products, such as CO₂, and water. Additional OH• is produced in the reaction between H₂O₂ and e⁻, further enhancing MB dye degradation [29–31].

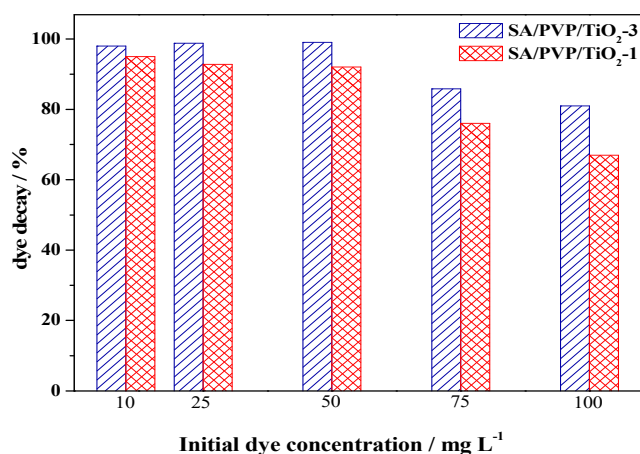


Figure 7. Effect of the initial concentration of MB dye on its photocatalytic decay using the nanocomposite beads (pH: 7; contact time: 120 min; light intensity: 1200 lm).

For higher values of initial MB dye concentration, the photocatalyst activity is diminished. This effect is likely related to a hampering of the reaction between OH• radicals and the dye molecules. As the initial dye concentration increases, the amount of MB molecules adsorbed onto the catalyst surface also increases, consequently hindering OH• formation [32]. Additionally, with the increase of color intensity, the gaps related to the photons entry are inhibited in reaching the photocatalyst surface, restraining the photodegradation of the dye by OH• radicals [31]. Herein, the optimum initial MB dye concentration was found to be 50 mg L⁻¹, with the SA/PVP/TiO₂-3 nanocomposite beads revealing a photodegradation efficiency of 98.9 %.

3.3. Reaction Kinetics Mechanism

3.3.1. Kinetic Models

The reaction mechanism between the SA/PVP/TiO₂ nanocomposite beads and MB is examined by making use of pseudo-first order and pseudo-second order kinetic models. The reaction rate is usually described by the kinetic model, whereas the dependence of the former on the reacting species concentration defines the reaction order [33,34]. The study involved carrying out experiments both in the dark and under light irradiation. Table 2 shows that there are clear differences between the two models in the dark and under irradiation of visible light. In the pseudo-second order model, the rate constant K_2 for SA/PVP/TiO₂-3 in dark mode is the highest, indicating the chemisorption nature of the MB adsorption process [35].

Table 2. Kinetic parameters determined for the pseudo-first order and pseudo-second order models.

Nanocomposite Material	Pseudo-First Order			Pseudo-Second Order	
	q_e mg g^{-1}	K_1 s^{-1}	R^2	K_2 $\text{g mg}^{-1} \text{s}^{-1}$	R^2
SA/PVP/TiO ₂ -1 in dark	71.4 ± 0.2	0.051 ± 0.001	0.96	0.0004 ± 10 ⁻⁵	0.91
SA/PVP/TiO ₂ -3 in dark	73.6 ± 0.1	0.059 ± 0.001	0.93	0.0005 ± 10 ⁻⁵	0.98
SA/PVP/TiO ₂ -1 in light	91.9 ± 0.3	0.036 ± 0.001	0.96	0.0003 ± 10 ⁻⁵	0.99
SA/PVP/TiO ₂ -3 in light	98.3 ± 0.1	0.038 ± 0.001	0.98	0.0004 ± 10 ⁻⁵	0.97

3.3.2. Proposed MB Decay Reaction Mechanism onto SA/PVP/TiO₂

The MB degradation mechanism begins with the adsorption of the dye on the surface of the nanocomposite by electrostatic interactions [36], followed by its photodegradation. At pH values of 3–7, the beads have a negative surface charge. In addition, TiO₂ contains terminal oxygen atoms that consequently increase the interaction between the beads' surface and nitrogen atoms in the MB molecules [1]. Under the irradiation of light, electron-hole pairs are formed in TiO₂ and the generated OH• and O₂•⁻ radicals are concentrated on the surface [34]. The MB dye is then degraded into smaller molecular fragments, such as CO₂, H₂O, and H⁺, by these hydroxyl radicals or superoxide ion radicals.

Table 3 compares the produced nanocomposite beads to other TiO₂-based nanocomposites that have previously been investigated for the elimination of various organic dyes in the water. When compared to previously reported nanocomposite beads, the removal effectiveness of the herein prepared SA/PVP/TiO₂-3 nanocomposite beads was almost higher than that of the other TiO₂-based composites, with the latter also presenting unfavorable synthesis methods and cost.

3.4. Reusability of SA/PVP/TiO₂ Nanocomposite

Five consecutive experimental runs were performed under optimal conditions using the same set of beads to evaluate the reusability of SA/PVP/TiO₂ nanocomposites as indicated in Figure 8, which permits the process to be considered a cost-effective degradation process for MB. The SA/PVP/TiO₂ nanocomposite beads were recovered and used five times by washing with 0.1 M HCl solution. The obtained data reveal that the MB decay efficiency remained practically unchanged as the cycle number increased. This result may be due to the stability of TiO₂ nanotubes in the SA/PVP polymer matrix.

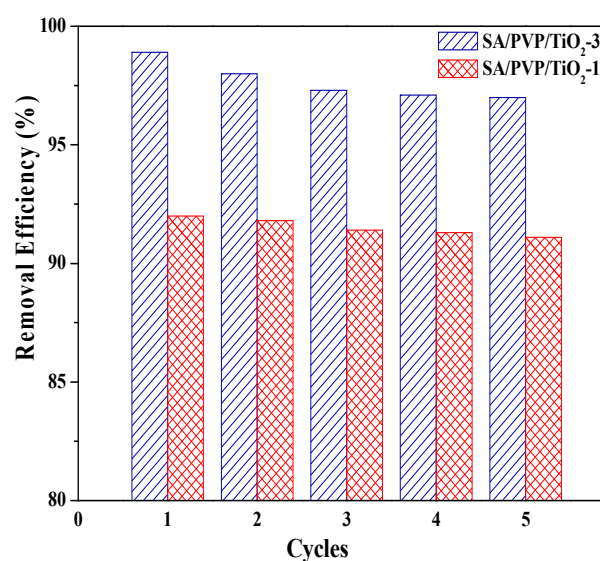
**Figure 8.** Reusability of SA/PVP/TiO₂ nanocomposites for the removal of MB during 5 consecutive cycles (at 120 min; pH 7; 50 mg L⁻¹ initial MB concentration).

Table 3. Photodegradation behavior towards organic dyes of different TiO₂-based composites.

Materials	TiO ₂ Morphology	Dye	Efficiency	Source
TiO ₂ embedded in SA/PVP nanocomposite beads	nanotube	methylene blue	up to 98.9%	this work
SA-TiO ₂ -bentonite	nanoparticles	methylene blue	90%	[37]
TiO ₂ immobilized in a Ca-alginate	nanoparticles	methylene blue	95%	[38]
TiO ₂ /Ca-alginate composite films	nanoparticles	methyl orange	82.2%	[14]
Acrylic acid-grafted SA-based TiO ₂ hydrogel nanocomposite	nanoparticles	methyl violet	99.6%	[15]
SA-TiO ₂ thin film	nanoparticles	Congo red	~59%	[16]
SA-TiO ₂ hybrid aerosol	nanoparticles	methyl orange	<85%	[39]
SA/carboxymethyl cellulose with nano-TiO ₂ and graphene oxide composite	nanoparticles	Congo red	98%	[40]

4. Conclusions

TiO₂ nanotubes were incorporated into a SA/PVP blend as a doping agent. The synthesized SA/PVP/TiO₂ nanocomposite beads were used to degrade MB dye in aqueous solutions when exposed to visible light irradiation using the concept of “absorb and degrade”. The process starts with the adsorption of the MB dye molecules on the surface of the SA/PVP/TiO₂ nanocomposite beads. Consequently, the adsorbed dye molecules undergo photocatalytic destruction by the TiO₂ nanotubes. The adsorption mechanism mainly depends on the porosity of the beads and the active sites on their surface, while the photocatalytic activity depends on the TiO₂. The determined MB removal profiles demonstrated that SA/PVP/TiO₂-3 nanocomposite beads perform better than SA/PVP/TiO₂-1 beads. Additionally, it was found that these nanocomposite beads may be easily recovered by simple washing and reused as effective tools for treating wastewaters contaminated with cationic dyes.

Author Contributions: Conceptualization, N.A.E.; methodology, M.H.G. and M.S.E.; formal analysis, A.H. and H.F.Z.; investigation, M.H.G., M.S.E., A.H. and H.F.Z.; writing—original draft preparation, N.A.E.; writing—review and editing, D.M.F.S.; visualization, M.M.A.E.-L.; supervision, M.M.A.E.-L.; project administration, M.M.A.E.-L. and D.M.F.S. All authors have read and agreed to the published version of the manuscript.

Funding: Fundação para a Ciência e a Tecnologia (FCT, Portugal) is acknowledged for a contract in the scope of programmatic funding UIDP/04540/2020 (D.M.F. Santos).

Data Availability Statement: The data presented in this study are available on request from the corresponding author.

Acknowledgments: The authors acknowledge the support from the City of Scientific Research and Technological Applications (SRTA-City), Alexandria, Egypt.

Conflicts of Interest: The authors declare no conflict of interest.

References

1. Elsayed, E.M.; Elnouby, M.S.; Gouda, M.H.; Elessawy, N.A.; Santos, D.M.F. Effect of the morphology of tungsten oxide embedded in sodium alginate/polyvinylpyrrolidone composite beads on the photocatalytic degradation of methylene blue dye solution. *Materials* **2020**, *13*, 1905. [[CrossRef](#)]
2. Eltaweil, A.S.; Abd El-Monaem, E.M.; Omer, A.M.; Khalifa, R.E.; Abd El-Latif, M.M.; El-Subruiti, G.M. Efficient removal of toxic methylene blue (MB) dye from aqueous solution using a metal-organic framework (MOF) MIL-101(Fe): Isotherms, kinetics, and thermodynamic studies. *Desalination Water Treat.* **2020**, *189*, 395–407. [[CrossRef](#)]
3. Mohy Eldin, M.S.; Gouda, M.H.; Abu-Saied, M.A.; Youssef, M.E.; El-Shazly, Y.M.S.; Farag, H.A. Removal of methylene blue by amidoxime polyacrylonitrile-grafted cotton fabrics: Kinetic, equilibrium, and simulation studies. *Fiber. Polym.* **2016**, *17*, 1884–1897. [[CrossRef](#)]
4. El Essawy, N.A.; Ali, S.M.; Farag, H.A.; Konsowa, A.H.; Elnouby, M.; Hamad, H.A. Green synthesis of graphene from recycled PET bottle wastes for use in the adsorption of dyes in aqueous solution. *Ecotox. Environ. Safe* **2017**, *145*, 57–68. [[CrossRef](#)] [[PubMed](#)]
5. Salama, A.; Mohamed, A.; Aboamera, N.M.; Osman, T.A.; Khattab, A. Photocatalytic degradation of organic dyes using composite nanofibers under UV irradiation. *Appl. Nanosci.* **2018**, *8*, 155–161. [[CrossRef](#)]

6. Sadettin, S.; Donmez, G. Bioaccumulation of reactive dyes by thermophilic cyanobacteria. *Process. Biochem.* **2006**, *41*, 836–841. [[CrossRef](#)]
7. Aksu, Z.; Tezer, S. Biosorption of reactive dyes on the green alga *Chlorella vulgaris*. *Process. Biochem.* **2005**, *40*, 1347–1361. [[CrossRef](#)]
8. Guibal, E.; Roussy, J. Coagulation and flocculation of dye-containing solutions using a biopolymer (Chitosan). *React. Funct. Polym.* **2007**, *67*, 33–42. [[CrossRef](#)]
9. Sarkar, S.; Chakraborty, S.; Bhattacharjee, C. Photocatalytic degradation of pharmaceutical wastes by alginate supported TiO₂ nanoparticles in packed bed photoreactor (PBPR). *Ecotox. Environ. Safe.* **2015**, *121*, 263–270. [[CrossRef](#)] [[PubMed](#)]
10. Kanakaraju, D.; Ravichandar, S.; Lim, Y.C. Combined effects of adsorption and photocatalysis by hybrid TiO₂/ZnO-calcium alginate beads for the removal of copper. *J. Environ. Sci.* **2017**, *55*, 214–223. [[CrossRef](#)]
11. Fujishima, A.; Honda, K. Electrochemical photolysis of water at a semiconductor electrode. *Nature* **1972**, *238*, 37–38. [[CrossRef](#)]
12. Luttrell, T.; Halpegamage, S.; Tao, J.; Kramer, A.; Sutter, E.; Batzill, M. Why is anatase a better photocatalyst than rutile? Model studies on epitaxial TiO₂ films. *Sci. Rep.* **2014**, *4*, 4043. [[CrossRef](#)]
13. Zhan, W.; Guo, Y.; Gong, X.; Guo, Y.; Wang, Y.; Lu, G. Current status and perspective of rare earth catalytic materials and catalysis. *Chin. J. Catal.* **2014**, *35*, 1238–1250. [[CrossRef](#)]
14. Zhao, K.; Feng, L.; Li, Z.; Fu, Y.; Zhang, X.; Wei, J.; Wei, S. Preparation, characterization and photocatalytic degradation properties of a TiO₂/calcium alginate composite film and the recovery of TiO₂ nanoparticles. *RSC Adv.* **2014**, *4*, 51321–51329. [[CrossRef](#)]
15. Thakur, S.; Arotiba, O. Synthesis, characterization and adsorption studies of an acrylic acid-grafted sodium alginate-based TiO₂ hydrogel nanocomposite. *Adsorpt. Sci. Technol.* **2018**, *36*, 458–477. [[CrossRef](#)]
16. Reveendran, G.; Ong, S.T. Application of experimental design for dyes removal in aqueous environment by using sodium alginate-TiO₂ thin film. *Chem. Data Collect.* **2018**, *15–16*, 32–40. [[CrossRef](#)]
17. Babu, V.R.; Sairam, M.; Hosamani, K.M.; Aminabhavi, T.M. Preparation of sodium alginate–methylcellulose blend microspheres for controlled release of nifedipine. *Carbohydr. Polym.* **2007**, *69*, 241–250. [[CrossRef](#)]
18. Akamatsu, K.; Maruyama, K.; Chen, W.; Nakao, A.; Nakao, S. Drastic difference in porous structure of calcium alginate microspheres prepared with fresh or hydrolyzed sodium alginate. *J. Colloid Interface Sci.* **2011**, *363*, 707–710. [[CrossRef](#)] [[PubMed](#)]
19. Mirzaie, Z.; Reisi-Vanani, A.; Barati, M. Polyvinyl alcohol-sodium alginate blend, composited with 3D-graphene oxide as a controlled release system for curcumin. *J. Drug Deliv. Sci. Technol.* **2019**, *50*, 380–387. [[CrossRef](#)]
20. Mary, C.S.; Swamiappan, S. Sodium alginate with PEG/PEO blends as a floating drug delivery carrier—In vitro evaluation. *Adv. Pharm. Bull.* **2016**, *6*, 435–442. [[CrossRef](#)]
21. Bhattacharyya, R.; Ray, S.K. Adsorption of industrial dyes by semi-IPN hydrogels of acrylic copolymers and sodium alginate. *J. Ind. Eng. Chem.* **2015**, *22*, 92–102. [[CrossRef](#)]
22. Gouda, M.H.; Gouveia, W.; Afonso, M.L.; Šljukić, B.; El Essawy, N.A.; Nassr, A.B.A.A.; Santos, D.M.F. Poly(vinyl alcohol)-based crosslinked ternary polymer blend doped with sulfonated graphene oxide as a sustainable composite membrane for direct borohydride fuel cells. *J. Power Sources* **2019**, *432*, 92–101. [[CrossRef](#)]
23. Gouda, M.H.; Gouveia, W.; Ellessawy, N.A.; Šljukić, B.; Nassr, A.B.A.A.; Santos, D.M.F. Simple design of PVA-based blend doped with SO₄(PO₄)-functionalised TiO₂ as an effective membrane for direct borohydride fuel cells. *Int. J. Hydrog. Energy* **2020**, *45*, 15226–15238. [[CrossRef](#)]
24. Habib, M.A.; Shahadat, M.T.; Bahadur, N.M.; Ismail, I.M.I.; Mahmood, A.J. Synthesis and characterization of ZnO-TiO₂ nanocomposites and their application as photocatalyst. *Int. Nano Lett.* **2013**, *3*, 5. [[CrossRef](#)]
25. Li, K.; Zhu, J.; Guan, G.; Wu, H. Preparation of chitosan-sodium alginate films through layer-by-layer assembly and ferulic acid crosslinking: Film properties, characterization, and formation mechanism. *Int. J. Biol. Macromol.* **2019**, *122*, 485–498. [[CrossRef](#)] [[PubMed](#)]
26. Ebrahimi, R.; Maleki, A.; Zandsalimi, Y.; Ghanbari, R.; Shahmoradi, B.; Rezaee, R.; Safari, M.; Joo, S.W.; Daraei, H.; Puttaiah, S.H.; et al. Photocatalytic degradation of organic dyes using WO₃-doped ZnO nanoparticles fixed on a glass surface in aqueous solution. *J. Ind. Eng. Chem.* **2019**, *73*, 297–305. [[CrossRef](#)]
27. Şahin, Ö.; Kaya, M.; Saka, C. Plasma-surface modification on bentonite clay to improve the performance of adsorption of methylene blue. *Appl. Clay Sci.* **2015**, *116*, 46–53. [[CrossRef](#)]
28. Dutta, D.; Thakur, D.; Bahadur, D. SnO₂ quantum dots decorated silica nanoparticles for fast removal of cationic dye (methylene blue) from wastewater. *Chem. Eng. J.* **2015**, *281*, 482–490. [[CrossRef](#)]
29. Abdelrahman, E.A.; Hegazey, R.M.; Kotp, Y.H.; Alharbi, A. Facile synthesis of Fe₂O₃ nanoparticles from Egyptian insecticide cans for efficient photocatalytic degradation of methylene blue and crystal violet dyes. *Spectrochim. Acta A Mol. Biomol. Spectrosc.* **2019**, *222*, 117195. [[CrossRef](#)]
30. Abdelrahman, E.A.; Hegazey, R.M. Facile synthesis of HgO nanoparticles using hydrothermal method for efficient photocatalytic degradation of crystal violet dye under UV and sunlight irradiation. *J. Inorg. Organomet. Polym. Mater.* **2019**, *29*, 346–358. [[CrossRef](#)]
31. Nassar, M.Y.; Aly, H.M.; Abdelrahman, E.A.; Moustafa, M.E. Synthesis, characterization, and biological activity of some novel Schiff bases and their Co(II) and Ni(II) complexes: A new route for Co₃O₄ and NiO nanoparticles for photocatalytic degradation of methylene blue dye. *J. Mol. Struct.* **2017**, *1143*, 462–471. [[CrossRef](#)]

32. Yang, Y.; Zhang, C.; Huang, D.; Zeng, G.; Huang, J.; Lai, C.; Zhou, C.; Wang, W.; Guo, H.; Xue, W.; et al. Boron nitride quantum dots decorated ultrathin porous g-C₃N₄: Intensified exciton dissociation and charge transfer for promoting visible-light-driven molecular oxygen activation. *Appl. Catal. B* **2019**, *245*, 87–99. [[CrossRef](#)]
33. Liu, Z.; Liu, R.; Yi, Y.; Han, W.; Kong, F.; Wang, S. Photocatalytic degradation of dyes over a xylan/PVA/TiO₂ composite under visible light irradiation. *Carbohydr. Polym.* **2019**, *223*, 115081. [[CrossRef](#)]
34. Liu, S.; Tang, W.; Chou, P. Microwave-assisted synthesis of triple 2D g-C₃N₄/Bi₂WO₆/rGO composites for ibuprofen photodegradation: Kinetics, mechanism and toxicity evaluation of degradation products. *Chem. Eng. J.* **2020**, *387*, 124098. [[CrossRef](#)]
35. Bhavsar, K.S.; Labhane, P.K.; Dhake, R.B.; Sonawane, G.H. Solvothermal synthesis of activated carbon loaded CdS nanoflowers: Boosted photodegradation of dye by adsorption and photocatalysis synergy. *Chem. Phys. Lett.* **2020**, *744*, 137202. [[CrossRef](#)]
36. Eltaweil, A.S.; Abd El-Monaem, E.M.; El-Subruiti, G.M.; Abd El-Latif, M.M.; Omer, A.M. Fabrication of UiO-66/MIL-101(Fe) binary MOF/carboxylated-GO composite for adsorptive removal of methylene blue dye from aqueous solutions. *RSC Adv.* **2020**, *10*, 19008–19019. [[CrossRef](#)]
37. Subekti, R.; Helmiyati, H. Sodium alginate-TiO₂-bentonite nanocomposite synthesis for photocatalysis of methylene blue dye removal. *IOP Conf. Ser. Mater. Sci. Eng.* **2020**, *763*, 012018. [[CrossRef](#)]
38. Albarelli, J.Q.; Santos, D.T.; Murphy, S.; Oelgemöller, M. Use of Ca-alginate as a novel support for TiO₂ immobilization in methylene blue decolorisation. *Water Sci Technol.* **2009**, *60*, 1081–1087. [[CrossRef](#)]
39. Dai, J.; Tian, Q.; Sun, Q.; Wei, W.; Zhuang, J.; Liu, M.; Cao, Z.; Xie, W.; Fan, M. TiO₂-alginate composite aerogels as novel oil/water separation and wastewater remediation filters. *Compos. Part. B Eng.* **2019**, *160*, 480–487. [[CrossRef](#)]
40. Thomas, M.; Natarajan, T.S.; Sheikh, M.U.D.; Bano, M.; Khan, F. Self-organized graphene oxide and TiO₂ nanoparticles incorporated alginate/carboxymethyl cellulose nanocomposites with efficient photocatalytic activity under direct sunlight. *J. Photochem. Photobiol. A Chem.* **2017**, *346*, 113–125. [[CrossRef](#)]